Nature, 441, doi:10.1038/nature04797, 968-971, 2006

Interseismic strain accumulation and the earthquake potential on the southern San Andreas fault system

Yuri Fialko

Institute of Geophysics and Planetary Physics, Scripps Institution of Oceanography, University of California San Diego, La Jolla, CA

submitted Sep. 2005; revised Mar. 2006; accepted Mar. 2006

The San Andreas fault (SAF) in California is a mature continental transform fault that accommodates a significant fraction of motion between the North American and Pacific Plates. The two most recent great earthquakes on the SAF ruptured its northern and central sections in 1906 and 1857, respectively. However, the southern section of the fault has not produced a great earthquake in historic times (over more than 250 years). Assuming the average slip rate of a few centimeters per year typical of the rest of the SAF, the minimum amount of slip deficit accrued on the southern SAF is of the order of 7-10 meters, comparable to the maximum co-seismic offset ever documented on the fault [1,2]. Here I present high-resolution measurements of interseismic deformation across the southern San Andreas fault system using a well-populated catalog of space-borne Synthetic Aperture Radar data. The data reveal a nearly equal partitioning of deformation between the southern San Andreas and San Jacinto faults, with a pronouced asymmetry in strain accumulation with respect to the geologically mapped fault traces. The observed strain rates confirm that the SAF is approaching the end of its interseismic recurrence.

The absence of great historic earthquakes on the southern SAF implies three possibilities. First, the fault may undergo a substantial creep, at least near the surface[3,4], similar to the central 40-km long fault section between Parkfield and San Juan Batista (see Figure S1 of the Supplementary materials). Second, the slip rate on the southern SAF may be significantly lower than the rate of 30-40 mm/yr measured elsewhere on the SAF[5], perhaps due to transfer of slip onto neighboring faults, in particular, the San Jacinto fault to the west of the SAF[6]. In this case, the seismic slip deficit on the southern SAF may be of the order of a few meters,

comparable to the present day slip deficits on the northern and central sections of the SAF. Third, the southern SAF may be accumulating elastic strain at a high (∼30 mm/yr) slip rate, and be late in the interseismic phase of the earthquake cycle. Distinguishing between these possibilities is important, as they have very different implications for the seismic hazard estimates. For example, due to a lack of significant (moment magnitude greater than 7) historic earthquakes on the southern SAF, and portions of the San Jacinto fault (e.g., the Anza gap), these faults are currently believed to pose the largest seismic risk in California [2,7]. Except for the first scenario, the continued quiescence increases the likelihood of a future event.

Different scenarios of strain accumulation and the likelihood of large future events on the southern SAF system may be ultimately discriminated with the help of precise spatially dense measurements of surface deformation. Previous studies have attempted to estimate the contemporaneous slip rates on the southern SAF system by fitting elastic halfspace models to rather sparse ground-based geodetic measurements from a dozen of monuments spanning a ∼100 km long profile across the fault[8,9]. Also, InSAR (Interferometric Synthetic Aperture Radar) data collected in the near field of the geologically mapped fault trace were used to detect the presence and extent of fault creep[4]. The far-field point measurements including GPS (Global Positioning System) and EDM (electronic distance measurements), as well as geologic data indicate that the southern SAF system accommodates a substantial fraction of the relative motion between the North American and Pacific plates, although the inferred slip rates vary greatly, from as low as 10 to as high as 35 mm/yr[6,10]. In this paper I investigate the interseismic strain accumulation on the southern SAF system using the the spatially and temporally dense InSAR data collected by the European Space Agency satellites ERS-1 and 2 between 1992 and 2000, and point measurements of surface velocities derived from the GPS and EDM data representing a time interval between 1985 and 2005.

Figure 1 shows the satellite line of sight (LOS) velocity, in millimeters per year, from the ERS track 356 covering the San Bernardino-Coachella Valley segment of the southern San Andreas fault. The average LOS velocities are derived from a stack of 35 radar interferograms. Details of the InSAR data processing and reduction are presented in the Supplementary material. To account for any residual error due to an imprecise orbit information, I

subtract the best-fitting linear trend (a planar "ramp") from the interferometric stack using independent data from more than 50 GPS stations located within the radar swath[11]. The remaining non-linear signal reveals gradual changes in the radar range that follow the strike of the San Andreas fault, and are consistent with the sense of motion between the North American and Pacific plates. Assuming that this signal is due to the surface motion, and that the motion is predominantly horizontal and parallel to a local strike of the SAF, the inferred LOS velocity of 13-14 mm/yr corresponds to the horizontal velocity of ∼45 mm/yr, in a good agreement with the plate tectonic models[12] and GPS measurements, but somewhat higher than the geologic estimates based on cumulative slip rates of major faults in southern California[6,13].

It is instructive to compare the InSAR data to independent point measurements of surface deformation from ground-based surveys. Figure 2 shows a comparison between the InSAR data from the A-A′ profile, and EDM and GPS measurements projected onto the satellite line of sight. Locations of the EDM and GPS monuments within the profile are indicated by the respective color symbols in Figure 1. To make a comparison more stringent, the GPS data were not used to remove a residual orbit error from the stacked InSAR data shown in Figure 2. Instead, the InSAR data were de-trended by fitting a plane to the north-eastern part of the interferogram that covers a presumably undeformed part of the North American plate (Figure 1). The best-fitting plane was then subtracted from the entire interferogram, effectively producing a map of LOS velocities with respect to the stable North America. As one can see from Figure 2, the InSAR data are in excellent agreement with the GPS and EDM measurements on both ends of the profile, yielding a total relative motion between the North American and Pacific plates in southern California at an average rate of 45 ± 2 mm/yr. All available geodetic data clearly indicate two major zones of high strain rate associated with the San Andreas and San Jacinto faults, and no significant strain accumulation due to the Elsinore fault.

A prominent feature of strain accumulation on the southern San Andreas and San Jacinto faults that was not recognized in the ground data[8,9] is a significant asymmetry in the velocity gradient with respect to the fault traces. In both cases, velocities on the eastern side of the faults are markedly higher than velocities on the western side. Such an asymmetry

is not expected for vertical strike-slip faults provided that the Earth's crust is transversely homogeneous and isotropic. Indeed, no simple dislocation models of interseismic strain accumulation are able to explain the space geodetic data shown in Figure 2 (see Figure S2). Possible explanations for the concentrated deformation on one side of a fault include across-fault contrasts in the effective shear modulus of the host rocks[14,15], postseismic relaxation in the presence of lateral variations in the effective viscosity of the substrate[16], multiple sub-parallel shear zones[17], and a non-vertical fault geometry[18,19]. Postseismic transients are an unlikely explanation given the large time lapse since the presumend last great earthquake on the southern SAF. To test the hypothesis of a rigidity contrast between rocks on different sides of the faults, I performed a number of theoretical simulations of interseismic strain accumulation on the San Andreas-San Jacinto fault system in the presence of lateral variations in the effective shear modulus of the crust. In these simulations I prescribe various slip rates, fault locking depths, and rigidity contrasts between the fault-bounded crustal blocks, and compute the resulting deformation at the Earth's surface. The faults are assumed to be vertical, and follow the geologically mapped traces; for the southern San Jacinto fault, this implies that its currently active branch is the Coyote Creek fault (Figure 1). Simulations are implemented using a finite element code ABAQUS. The computational domain is a parallepiped having dimensions of $200 \times 100 \times 30$ km representing the across-fault, depth, and along-fault coordinates, respectively. The interseismic loading is introduced by prescribing a constant strike-slip displacement on a deep extension of the San Andreas and San Jacinto faults. The red line in Figure 2 shows theoretical LOS velocities from the best-fitting model. The best-fitting model suggests the slip rate of 25 mm/yr and the locking depth of 17 km for the southern San Andreas fault, and 21 mm/yr and 12 km, respectively, for the San Jacinto fault. For both faults, the shear modulus of the western side of the fault is inferred to be three times larger than the shear modulus of the eastern side. There is a certain trade-off between the assumed slip rates, fault locking depths, and the rigidity contrasts. Based on a number of simulations, the estimated uncertainty in the fault slip rate is 2-3 mm/yr, and the uncertainty in the fault locking depth is 2-4 km. The data require a contrast in the elastic modulus of at least a factor of two, and much higher contrasts (e.g., a factor of five) cannot be ruled out. Note that there is some disagreement between the campaign-mode GPS and

EDM data from the SCEC velocity model, on one hand, and the InSAR data and continuous SCIGN GPS data, on the other hand, on the eastern side of the SAF. The SCEC data seem to suggest somewhat lower slip rate and thickness of the brittle layer compared to the InSAR and SCIGN GPS data. This disagreement is unlikely due to vertical deformation, as the latter would imply subsidence to the east of the fault. Taking the SCIGN GPS measurements of vertical motion at face value, the data indicate uplift, rather subsidence, to the east of the fault trace. A good agreement between the InSAR data and well-constrained horizontal velocity from the SCIGN GPS data (see a black triangle at ∼105 km along the profile A-A′ in Figure 2) argues for little, if any vertical deformation to the east of the fault. Because the best-fitting model is a compromise between all available geodetic data, the deduced slip rate and the rigidity contrast on the southern SAF should be considered lower bounds.

Asymmetric patterns of interseismic velocities have been reported elsewhere on the SAF and other major strike-slip faults[15,20,21], and often attributed to lateral variations in crustal rigidity[14,15]. Significant (a factor of two) variations in the effective shear modulus were also reported for kilometer-wide damage zones around several faults in southern California [11,22]. Variations in the effective elastic properties of the Earth's crust across mature faults are perhaps not surprising, as large-offset faults often juxtapose terrains with dissimilar compositions and mechanical properties[23]. However, the inferred magnitude of the rigidity contrasts exceeds high-end estimates from seismic tomography of a factor of 2-2.5[24,25]. The total inferred contrast across the San Andreas and San Jacinto faults is about a factor of 5 to 10, significantly larger than any seismically determined lateral variations in elastic moduli, but comparable to inferences based on geodetic data from other localities[15]. An alternative possibility is that the Quaternary fault traces are not indicative of the fault positions below the brittle layer. To explore this possibility, I hypothesise that the Coyote Creek fault is not the main branch of the southern San Jacinto fault system, and that most of strain accumulation occurs on an unmapped strike-slip fault connecting the southern termination of the San Jacinto fault and the Superstition Hills fault (see dashed red line in Figure 1). In case of the SAF, one might argue that the fault is dipping to the east [26,27], based on a fact that seismicity occurs several kilometers off the fault trace[28]. The hypothesised alternative locations of shear zones driving the interseismic deformation at

the brittle-ductile transition are denoted by dashed green lines in Figure 2. Under these assumptions, it is possible to explain the data equally well without appealing to variations in the effective shear modulus of the crust (see dashed red line in Figure 2). In this case, the inferred slip rates are 25 and 19 mm/yr, and the locking depths are 12 and 10 km for the San Andreas and San Jacinto faults, respectively. The assumed position of the southern San Jacinto fault (Figure 1) is supported by a lineament of microseismicity[28], yet the absence of an active fault trace is puzzling. Partly, such absence might be explained by alluvial burial from the ancient Lake Cahuilla[29]. However, it is not clear whether the corresponding fault segment remained quiescent over 400 years since the lake retreat[29], or could be a "blind" strike-slip fault[19]. For the San Andreas fault, the fault dip angle required by the homogeneous model is $\sim 30^\circ$ off vertical. A steeper fault implies a greater rigidity contrast. Ultimately, the proposed interpretations of interseismic strain accumulation admit a robust observational test. The rigidity contrast model predicts that if future major earthquakes occur on subvertical ruptures coincident with the mapped traces of the San Andreas and San Jacinto faults, the resulting coseismic displacement field should be essentially asymmetric, with displacements on the eastern side of a fault being at least two to three times larger than displacements on the western side of a fault. Ruptures having the proposed alternative fault geometries will be a direct evidence against large rigidity contrasts. These results suggest that, in general, information about coseismic deformation on a given fault, such as asymmetries in the radiation pattern, and static displacement fields[18,27] may greatly reduce uncertainties in interpretation of the interseismic deformation data.

Regardless of details of fault geometry and mechanical properties of the ambient crust, results presented in this study lend support to intermediate-term forecasts of a high probability of major earthquakes on the southern San Andreas fault system[2,7]. Space geodetic data shown in Figures 1 and 2 clearly demonstrate that the southern SAF is accumulating significant elastic strain, as indicated by a broad area of high gradients in the LOS velocity field on the eastern side of the fault. While some creep may be occurring in the uppermost crust[4], as evidenced by a steep gradient in the LOS velocity immediately to the west of the surface trace of the SAF (see Figure 2), it does not prevent (and if anything, enhances) a build-up of tectonic stress on the rest of the fault at seismogenic depths. I point out that the step-like

increase in the radar range across the SAF may not be entirely due to right-lateral fault creep, and likely involves ground subsidence to the west of the fault. Without subsidence, the observed variations in the LOS velocity would imply left-lateral deformation within the decorrelated area and immediately to the west of Salton Sea (at ∼120-130 km along the profile A-A′, see Figure 2), which is highly unlikely. The inferred ground subsidence may be either man-made (e.g., due to agricultural activities in the Coachella Valley), or of tectonic origin (e.g., indicating secular deepening of the Salton Trough). While it might be possible to discriminate between the horizontal and vertical components of deformation using complementary InSAR data from ascending orbits, unfortunately no suitable acquisitions are available.

The current slip rate on the southern SAF of 25 ± 3 mm/yr determined from the space geodetic data is in excellent agreement with some long-term geologic estimates (e.g., 25 ± 4 mm/yr[13]), although other geologic studies may suggest lower rates[10]. The discrepancy between different geologic datasets might be due to the along-fault variations in the mechanical behavior of the uppermost crustal layer. For example, zones of the apparently low slip rates might represent substantial inelastic yielding of a shallow layer in the interseismic period, either in the form of creep[4], or more distributed failure[19]. It is reasonable to assume that the geodetically determined slip rate remained relatively constant in the recent geologic past, and, in particular, over the last several hundred years. It follows that the relative seismic quiescence of the southern SAF over the last 250 years implies a slip deficit of 5.5 to 7 meters. This may be compared to paleoseismologic estimates of average recurrence times of large events on the southern SAF of 200-300 years, and average coseismic displacements of 4 to 7 meters[1,2]. Although simple time- and size-predictable earthquake models have been shown to be inadequate[30–32], and the repeat interval between large earthquakes may vary significantly, it may be argued that the accumulated slip deficit cannot greatly exceed the maximum coseismic offset documented throughout the fault history. If so, the southern SAF is likely in the late phase of its interseismic recurrence[2,7,9].

The data and modeling results presented in this study also reveal a surprisingly robust strain accumulation on the San Jacinto fault. The inferred slip rate on the San Jacinto fault of 19-21 mm/yr is significantly higher than most current estimates, but is in a good

agreement with geologic data representing average slip rates over $10^5 - 10^6$ yr time scales[6,33]. The lower (10-12 mm/yr) geodetic slip rates on the San Jacinto fault inferred from previous GPS studies may be in part due to the use of homogeneous elastic halfspace models (as well as assumed fault locations, see Figures 2 and S2) for the data interpretation. The spatially dense InSAR data demonstrates that the total slip rate on the SAF-San Jacinto system of 45 mm/yr is nearly equally partitioned between these two faults (Figures 1 and 2). Together, the San Jacinto and the southern San Andreas faults appear to accommodate the bulk of the relative motion between the North American and Pacific plates in southern California. These results imply little, if any deformation on other major crustal faults to the west of San Jacinto.

It should be noted that although the highly accurate and detailed geodetic data provide useful constraints on the rate of the interseismic build-up of stress, and the probability of large events on a given fault, the relationships between the loading rate, the absolute stress level, and the rate of seismicity are still poorly understood. For example, the low slip rate Elsinore fault is expressed in significant microseismicity. Intense microseismicity is also associated with the faster moving San Jacinto, while the SAF characterized by the highest slip rate is practically devoid of microearthquakes[25,28]. These patterns exemplify extremely complex relationships between the tectonic loading rate and seismic activity.

References

[1] Sieh, K., Stuiver, M. & Brillinger, D. A more precise chronology of earthquakes produced by the San Andreas fault in Southern California. *J. Geophys. Res.* **94**, 603–623 (1989).

[2] Weldon, R. J., Fumal, T. E., Biasi, G. P. & Scharer, K. M. Geophysics - Past and future earthquakes on the San Andreas fault. *Science* **308**, 966–967 (2005).

[3] Turcotte, D. L. & Schubert, G. *Geodynamics, 2nd ed.* 456 pp., Cambridge Univ., New York, NY, (2002).

[4] Lyons, S. & Sandwell, D. Fault creep along the southern San Andreas from interferometric synthetic aperture radar, permanent scatterers, and stacking. *J. Geophys. Res.* **108**, 10:1029/2002JB001831 (2003).

[5] Thatcher, W. & Lisowski, M. Long-term seismic potential of the San-Andreas fault southeast of San-Francisco, California. *J. Geophys. Res.* **92**, 4771–4784 (1987).

[6] Bennett, R. A., Friedrich, A. M. & Furlong, K. P. Codependent histories of the San Andreas and San Jacinto fault zones from inversion of fault displacement rates. *Geology* **32**, 961–964 (2004).

[7] Working Group on California Earthquake Probabilities. Seismic hazards in southern California: Probable earthquakes, 1994-2024. *Bull. Seism. Soc. Am.* **85**, 379–439 (1995).

[8] Johnson, H. O., Agnew, D. C. & Wyatt, F. K. Present-day crustal deformation in southern California. *J. Geophys. Res.* **99**, 23951–23974 (1994).

[9] Bennett, R. A., Rodi, W. & Reilinger, R. E. Global positioning system constraints on fault slip rates in southern California and northern Baja, Mexico. *J. Geophys. Res.* **101**, 21943–21960 (1996).

[10] der Woerd J., V., Klinger, Y., Sieh, K., Tapponnier, P. & Ryerson, F. Long-term slip rate of the southern San Andreas Fault, from ^{10}Be-^{26}Al surface exposure dating of an offset alluvial fan. *J. Geophys. Res.* , in press (2006).

[11] Fialko, Y. Probing the mechanical properties of seismically active crust with space geodesy: Study of the co-seismic deformation due to the 1992 M_w7.3 Landers (southern California) earthquake. *J. Geophys. Res.* **109**, B03307, 10.1029/2003JB002756 (2004).

[12] DeMets, C., Gordon, R. G., Argus, D. F. & Stein, S. Current plate motions. *Geophys. J. Int.* **101**, 425–478 (1990).

[13] Weldon, R. J. & Sieh, K. E. Holocene rate of slip and tentative recurrence interval for large earthquakes on the San Andreas fault, Cajon Pass, southern California. *Geol. Soc. Am. Bull.* **96**, 793–812 (1985).

[14] Lisowski, M., Savage, J. & Prescott, W. H. The velocity field along the San Andreas fault in central and southern California. *J. Geophys. Res.* **96**, 8369–8389 (1991).

[15] Le Pichon, X., Kreemer, C. & Chamot-Rooke, N. Asymmetry in elastic properties and the evolution of large continental strike-slip faults. *J. Geophys. Res.* **110**, Art. No. B03405 (2005).

[16] Li, V. C. & Rice, J. Crustal deformation in great California earthquake cycles. *J. Geophys. Res.* **92**, 11533–11551 (1987).

[17] Kenner, S. & Segall, P. Lower crustal structure in Northern California: Implications from strain rate variations following the 1906 San Francisco earthquake. *J. Geophys. Res.* **108**, 2011, doi:10.1029/2001JB000189 (2003).

[18] Fialko, Y., Simons, M. & Agnew, D. The complete (3-D) surface displacement field in the epicentral area of the 1999 M_w7.1 Hector Mine earthquake, southern California, from space geodetic observations. *Geophys. Res. Lett.* **28**, 3063–3066 (2001).

[19] Fialko, Y., Sandwell, D., Simons, M. & Rosen, P. Three-dimensional deformation caused by the Bam, Iran, earthquake and the origin of shallow slip deficit. *Nature* **435**, 295–299 (2005).

[20] Prescott, W. H. & Yu, S. B. Geodetic measurement of horizontal deformation in the Northern San Francisco Bay region, California. *J. Geophys. Res.* **91**, 7475–7484 (1986).

[21] Freymueller, J. T., Murray, M. H., Segall, P. & Castillo, D. Kinematics of the Pacific North America plate boundary zone, northern California. *J. Geophys. Res.* **104**, 7419–7441 (1999).

[22] Fialko, Y. *et al.* Deformation on nearby faults induced by the 1999 Hector Mine earthquake. *Science* **297**, 1858–1862 (2002).

[23] Thatcher, W. Microplate versus continuum description of active tectonic deformation. *J. Geophys. Res.* **100**, 3885–3894 (1983).

[24] Ben-Zion, Y. & Andrews, D. J. Properties and implications of dymanic rupture along a material interface. *Bull. Seismol. Soc. Am.* **88**, 1085–1094 (1998).

[25] Hauksson, E. Crustal structure and seismicity distribution adjacent to the Pacific and North America plate boundary in southern California. *J. Geophys. Res.* **105**, 13875–13903 (2000).

[26] Yule, D. & Sieh, K. Complexities of the San Andreas fault near San Gorgonio Pass: Implications for large earthquakes. *J. Geophys. Res.* **108**, 10.1029/2001JB000451 (2003).

[27] Fialko, Y., Rivera, L. & Kanamori, H. Estimate of differential stress in the upper crust from variations in topography and strike along the San Andreas fault. *Geophys. J. Int.* **160**, 527–532 (2005).

[28] Richards-Dinger, K. & Shearer, P. Earthquake locations in southern California obtained using source specific station terms. *J. Geophys. Res.* **105**, 10939–10960 (2000).

[29] Waters, M. R. Late Holocene lacustrine chronology and archaeology of ancient lake Cahuilla, California. *Quaternary Research* **19**, 373–387 (1983).

[30] Murray, J. & Segall, P. Testing time-predictable earthquake recurrence by direct measurement of strain accumulation and release. *Nature* **419**, 287–291 (2002).

[31] Weldon, R. J., Scharer, K. M., Fumal, T. E. & Biasi, G. P. Wrightwood and the earthquake cycle: What a long recurrence record tells us about how faults work. *GSA Today* **14**, 4–10 (2004).

[32] Cisternas, M. *et al.* Predecessors of the giant 1960 Chile earthquake. *Nature* **437**, 404–407 (2005).

[33] Sharp, R. V. San Jacinto fault zone in the Peninsular Ranges of southern California. *Geol. Soc. Am. Bull.* **78**, 705–730 (1967).

Acknowledgments. I thank Ray Weldon, Paul Segall, and an anonymous reviewer for useful suggestions. This work was supported by NSF (EAR-0450035) and the Southern California Earthquake Center (SCEC). Original InSAR data are copyright of the European Space Agency, distributed by Eurimage, Italy, and acquired via the WInSAR Consortium. The ERS SAR imagery was processed using the JPL/Caltech software package ROI_PAC. The continuous GPS data were provided by the Scripps Orbit and Permanent Array Center (SOPAC), and the campaign GPS and EDM data were provided by the Crustal Motion Model v3 of SCEC.

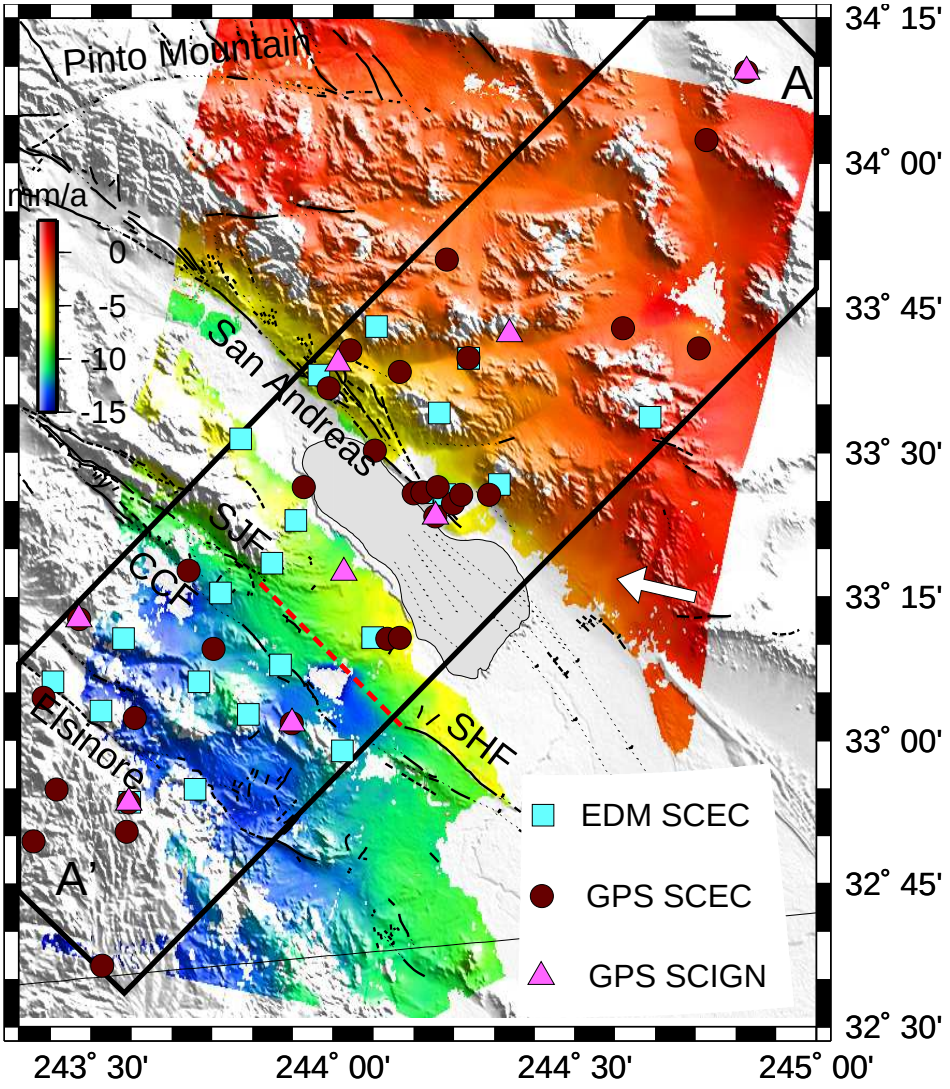

Figure 1: (1) Line of sight velocity of the Earth's surface from a stack of radar interferograms spanning a time interval between 1992 and 2000. The velocity map is draped on top of shaded topography. LOS velocities toward the satellite are assumed to be positive. White arrow shows the radar look direction. Black wavy lines denote Quaternary faults (SJF - San Jacinto fault, CCF - Coyote Creek fault, SHF - Superstition Hills fault). Red dashed line shows a hypothesised location of an active southern branch of the San Jacinto fault. Black box outlines a profile from which the InSAR and GPS data are extracted for a comparison and modeling (Figure 2). Color symbols denote positions of the GPS and EDM sites within the profile. Data from these sites are provided by the Southern California Earthquake Center (SCEC) and Southern California Integrated GPS Network (SCIGN).

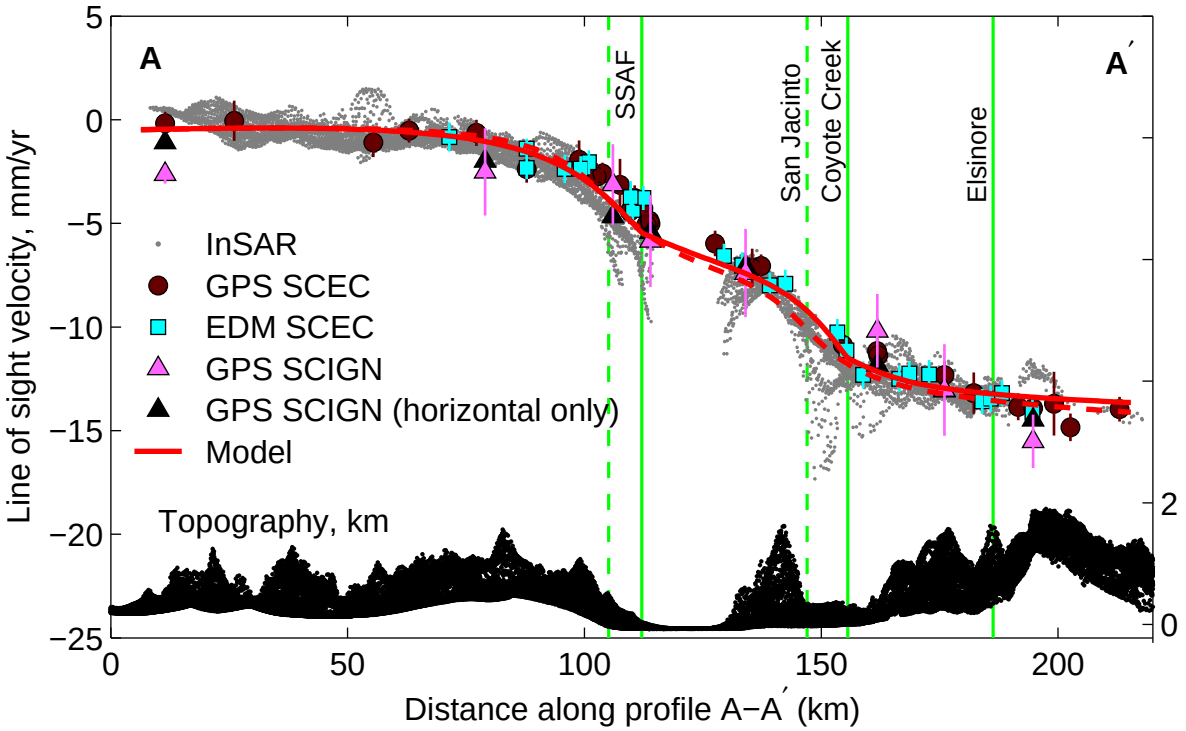

Figure 2: (2) Average LOS velocities (gray dots) and GPS/EDM data (color symbols) projected onto the satellite line of sight from a profile shown in Figure 1. Vertical bars denote the 2σ errors of the point measurements. Solid vertical lines denote positions of the mapped fault traces (solid lines), and hypothetical positions of interseismic creep at the bottom of the brittle layer (dashed lines). Solid red line is a theoretical model of interseismic strain accumulation due to a deep slip below the mapped traces of the San Andreas and San Jacinto faults in the presence of lateral variations in the crustal rigidity. Dashed red line is a theoretical model for the inferred alternative fault positions, assuming no lateral variations in the rock rigidity.